Aggregate Open Access WILEY

Large-Scale Chiral Spherulites with Controllable Circularly Polarized Luminescence in Liquid Crystal Block Copolymers Film

Jianan Yuan [2], Xuemin Lu [1]*, Qinghua Lu [1]*

[1] School of Chemistry and Chemical Engineering, Shanghai Jiao Tong University, Shanghai, 200240, China.
[2] School of Chemical Science and Engineering, Tongji University, Shanghai, 200092, China.
*E-mail: xueminlu@sjtu.edu.cn, qhlu@sjtu.edu.cn

Abstract

Macroscopic chiral spherulites prepared by hierarchical self-assembly have attracted considerable attention due to their excellent property as chiroptical materials. However, preparing controllable handedness spherulites in bulk film remains a challenge due to the absent knowledge of the evolution mechanism from the molecule to macroscopic crystal during chiral assembly. In this contribution, we constructed chiral controllable macroscopic spherulites with circularly polarized luminescence (CPL) using enantiomeric tartaric acid and Rhodamine B co-assembled with liquid crystal block copolymers, poly (ethylene oxide)-b-poly (methyl methacrylate) bearing azobenzene group side chains. It was found that the chiral liquid crystal field induced by exogenous chiral molecules was closely related to the formation of macroscopic chiral spherulites. Moreover, the transformation of azobenzene cis-trans isomerization under photo-thermal endows films with adjustable CPL. This facile strategy provides a platform to design large-scale chiral structures for chiroptical switching, encryption, and memory storage materials.

Keywords: macroscopic chirality, block copolymer, self-assembly, circularly polarized luminescence

1. Introduction

Among the chiral-assembled architectures found in nature, helix is probably the most captivating structure. Insect cuticles with cholesteric-phase periodic helical structures exhibit diverse colors in the presence of light,[1] and proteins with multi-level helical structures play a

crucial coordinating role in physiological processes.[2, 3] In addition, macroscopic chiral structures exhibit significant sensitivity and responsiveness to the external environment, such as the helical growth of cucumber tendril.[4] To achieve macroscopic chiral structures and their specific functions in biological systems, hierarchical chiral assembly has been developed to construct multidimensional large-scale chiral structures, including helical fibers [5] or ribbons, [6] chiral flowers,[7, 8] spiral tubes,[9] and chiral spherulites.[10] Then, multifunctional materials with chiral response have been prepared by introducing fluorescent molecules or other functional molecules *in situ* into the chiral structures, which exhibit significant applications in the fields of biological probes and signatures,[11] chiral metamaterials,[12, 13] flexible film,[14, 15] and three-dimensional optical displays.[16, 17]

In particular, chiral spherulites (including band spherulites), as a common morphology of crystalline polymers, are extensively exploring credit to their diverse crystal morphology which has a tremendous impact on material properties.[18] In general, the formation of chiral spherulites is attributed to lamellar crystal twisting along the radial growth direction.[19] For chiral crystalline polymers, the growth of lamellar crystals results in imbalanced stress on the surface of chain segments due to chirality, leading to periodic twisting of the lamellae for stress balance.[20-22] Maillard et al.[23] revealed the process of intramolecular chiral information transfer in chiral poly(lactic acid) (PLA) homopolymer systems and found that the lamellae twist of chiral PLA with a specific orientation, PLLA is *S*-shaped, while PDLA is *Z*-shaped. Similarly, using chiral molecules to induce achiral homopolymers, poly(2-vinylpyridine), resulted in the intermolecular chiral transfer and subsequently led to the formation of well-defined directional chiral band spherulites.[24] These results demonstrate the indispensable role of molecular chirality in the formation of macroscopic helical structures. Nevertheless, the mechanism of evolution from the molecular level to macroscopic spherulites remains ongoing discussed.

Block copolymers (BCPs), composed of two or more blocks with different physicochemical properties, have been intensively investigated because of their propensity for microphase separation-induced morphology. When endowing the blocks with chirality and the introduction of functional particles enables constructing the stimuli-responsive multiscale chiral structures.[25, 26] Ho et al.[27] reported the preparation of band spherulites by self-assembly of chiral block copolymer PS-*b*-PLLA, where the amorphous PS dispersed phase enhances the surface imbalanced stress, thus increasing the lamellae distortion rate and improving chiral band spherulites. Han et al.[28] demonstrated that the proportion of chiral blocks and the crystallization temperature are the essential factors in enhancing the distortion of lamellae and hence the formation of band spherulites. Interestingly, the introduction of conjugated fluorescent molecules into the chiral PLA not only imparts luminescent properties to the chiral films, but the macroscopic chiral structure exhibits a distinct spiral phenomenon due to the three-dimensional structural asymmetry.[29] These results are an indispensable guide to the exploration of chiral transfer and the construction of macroscopic-scale spiral crystals. In recent years, the chiral assembly of polymers induced by exogenous chiral molecules has been extensively investigated due to its universality and expandability compared to the traditional intrinsic chiral polymer self-assembly, especially as functional template for circularly polarized fluorescence (CPL) materials.[30, 31] However, the construction of large-scale spiral crystals with controllable handedness and luminescence in exogenous chiral environments remain a challenge.

Herein, we report a multi-component co-assembly method to fabricate the large-scale spiral spherulites with chiroptical switches in an achiral liquid crystal block copolymer (LC-BCP) **(Scheme 1)**. Chiral tartaric acid (TA) molecules, achiral LC-BCP, and fluorescent molecules (Rhodamine B, RhB) were co-assembled under the liquid crystalline temperature (125 ℃) to prepare handedness-controllable spherulite films. The chiral transfer between TA, RhB, and LC-BCP was achieved through non-covalent interaction, which was demonstrated at

the molecular level using chiral spectroscopy. Also, controllable chiral structures were shown at macroscale, which was confirmed using electron and optical microscopy. Moreover, the fluorescent molecules were induced to a helical arrangement by the chiral template and the film displayed orange CPL under 530 nm excitation, g_{lum} up to 0.02. Based on the transformation of the cis-trans isomerization of azobenzene, the fluorescence of the film can be erased under UV excitation and recovered after thermal annealing. This controllable chiral assembly is a facile method for the preparation of large-scale chiral spherulites and provides an elegant strategy for the construction of chiroptical materials.

2. Result and discussion

2.1 Morphology characterization of three-dimensional spiral spherulites

Three-dimensional spiral spherulites with defined direction in LC-BCP/TA/RhB film were observed using polarized optical microscopy (POM) and 3D microscope, D-TA induced chiral assembly to obtain clockwise spiral spherulites (**Figure 1a, c**), while counterclockwise spiral spherulites at L-TA **(Figure 1b, d)**. First, we monitored the growth process of spherulites using POM. When the film was annealed for 1 min, some small crystals appeared, indicating the initial stage of crystal nucleation. As the annealing time prolonged (5min), the crystal growth process was promoted and these spherulites assemblies rapidly grew into larger-size spherulites with slightly directional rotational behavior. After 15 min annealing, the macroscopic spherulite morphology stopped growth due to space constraints.[32] Eventually, a macroscopic spheroidal morphology was formed at 1 h **(Figure S1)**. Notably, the rotation of the spherulites was significantly amplified during the growth process and the scale of spherulites can reach up to 1 mm.

In general, chiral polymer spherulites do not exhibit distinct macroscopic rotational behavior, even for banded spherulites induced by chain tilting in lamellae.[33] Therefore, we further discussed the constituents of the spherulites and the origin of the spiral behavior by designing model compounds, PEO, PMA (Azo), TA and RhB assemblies. As shown in **Figure**

S2a, neat D-TA or L-TA shows a spherulite morphology, but no macroscopic torsion appeared. The crystal morphology of the TA/RhB assemblies is similar to the neat TA molecule, showing a conventional spherulite structure (**Figure S2b**). However, the differential scanning calorimetry (DSC) curve of TA/RhB complex shows only one melt peak (168 °C), which is significantly different from the melt peaks of TA (175 °C) and RhB (210 °C). Thus, it can be speculated that the crystal corresponding to this melt peak is a eutectic of TA and RhB molecules. When observing the PEO/TA/RhB composite film, it was found that the spherulite structure was irregular and smaller in scale (**Figure S2c**). The DSC curves show that PEO is a crystalline polymer, but the hydrogen bonding interaction between the TA and PEO leads to a decrease in the crystalline properties of PEO [34] and the formation of amorphous regions inhibit TA/RhB crystallization. This result is also supported by the broadening of the melting peak at 166 °C corresponding to the TA/RhB in the DSC heating curve of PEO/TA/RhB (**Figure S2c**). The crystal structure of LC-BCP/RhB/TA was further investigated using wide-angle X-ray diffraction (WAXRD). As shown in **Figure 1e**, in the curve of neat LC-BCP, the peaks at 19 ° and 21 ° are attributed to the crystallization peaks of the PEO segments. After doping with TA, the crystallization of PEO is inhibited by the hydrogen bond between TA and PEO, and found a broad diffraction peak (16.5°), which is consistent with the above DSC results. After further mixing with RhB, part of the diffraction peaks of TA disappeared and new peaks were found at 28°, 35°, and 38°, indicating a new molecular arrangement of TA/RhB/LC-BCP film. Although, the TA, TA/RhB and PEO/TA/RhB crystals have a chiral component, there is no chiral distortion behavior in the macrostructures (**Figure S2**). While, the effect of the liquid crystal homopolymer PMA (Azo) on the TA/RhB eutectic was significantly different from the above results. After isothermal crystallization of the PMA (Azo)/TA/RhB composite films at the liquid crystal state temperature (120 °C) for 5 min, spherulites with a clear rotational direction were observed, with D-TA showing clockwise and L-TA showing counterclockwise, consistent with the block copolymer system (**Figure S3**). According to previous reports,[35] chiral TA

induces the formation of chiral liquid crystal fields through hydrogen bonding interactions with PMA (Azo), so it is reasonable to assume that chiral liquid crystal fields drive spherulites torsion in this case.

To verify this assumption, the effect of crystallization temperature on the morphology of spiral spherulite (LC-BCP/TA/RhB) was investigated using DSC and POM. A 60 μL solution of LC-BCP/TA/RhB was drop-coated on a silicon wafers, and after evaporation of THF, the samples were isothermally annealed for 5 min at 25 °C, 60 °C, 90 °C, 100 °C, 110 °C, 125 °C, 160 °C and 180 °C, respectively. As shown in **Figure 2**, diverse spherulite structures were observed at different crystallization temperatures. From the DSC curves and POM images of the composite films, the polymer chain segments are in the glassy state at 25 °C, but the TA-induced polymer banded spherulites were still observed due to the high TA molecular content (50 wt.%). When the crystallization temperature increased to 60 °C, the PEO chain segments moved affecting the TA-induced crystallization. On the other hand, RhB and TA form eutectic resulting in the transformation of spherulites. However, no rotation of the crystal is observed. Increasing the crystallization temperature to 90 °C, a twisting phenomenon in the spherical crystal structure appeared. We also found that the composite films annealed at 100 °C, 110 °C, and 125 °C all showed macroscopic spiral spherulite. This is due to the composite films being in the liquid crystal state at 90 °C, 100 °C, 110 °C and 125 °C, and the polymer chain segments move in an orderly manner, resulting in difference in the morphology of crystals. To further verify the importance of liquid crystals on the spiral behavior of spherulite, the composite films were annealed at isotropic temperature of LC-BCP and obtained non-twisted spherical crystals (160 °C) and crystal-free images (180 °C). These results demonstrated that the PMA(Azo) liquid crystal blocks play an indispensable role in the formation of spiral crystals. In addition, the effect of chiral factors and component ratios on the formation of spherical crystals is also discussed. As shown in **Figure S4**, there is no crystallization occurring in those films without TA. On the one hand, this phenomenon demonstrated the importance of chiral TA

crystallization promoters, on the other hand, the confining effect of polymer domains on the crystallization of small molecules. As shown in **Figure S5**, the LC-BCP/TA films without RhB molecules showed only the banded spherulites. The size of the spherulites increases as the proportion of RhB molecules decreases, suggesting that RhB molecules are an important component in the assembly of spiral spherulite, but not the factor controlling the orientation. Overall, the spiral spherulites (macroscopic chiral morphology) are constructed under temperature annealing in the liquid crystal state and the molecular chirality determines the rotating direction of the macroscopic chiral assemblies. Although, spiral spherulites can be obtained in both liquid crystal homopolymer and LC-BCP system. However, in terms of scale and torsion, block copolymer assemblies are significantly higher and stronger than homopolymer systems. (**Figure 2 and Figure S3**). It is well known that block copolymers can self-assemble into ordered structures by microphase separation after thermal annealing. This variability in chiral geometry is closely related to the induction of ordered helical assembly by hierarchical chiral transfer.

2.2 Mechanism of hierarchical chiral transfer and assembly

To gain a deep insight into the chiral transfer process at the molecular-conformation-phase level in the block copolymer system, the interactions between LC-BCP, TA, and RhB were investigated in detail. The molecular chirality of LC-BCP/TA/RhB annealed films was recorded using circular dichroism (CD). As shown in **Figure 3a**, a mirror signal at 218 nm was attributed to TA molecular chirality and a cotton effect at 259-489 nm, which corresponded to the characteristic adsorption of azobenzene groups. Significantly, the UV absorption peak at 570 nm corresponding to the conjugated structure of RhB also shows a mirror signal, suggesting induced chirality of RhB. These results indicated the occurrence of chiral transfer from TA to LC-BCP and RhB. There are two possible approaches for chiral transfer from TA to RhB: one is through direct interaction between chiral TA and RhB, the other is the induction of RhB helical arrangement by the chiral assembly of block copolymers. To elucidate the chiral

interaction, we compared the CD spectra of TA and TA/RhB assemblies (**Figure S6a and S6b**). The chiral signal of TA in the CD spectrum of TA/RhB was significantly red-shifted (218 nm) compared to the neat TA (212 nm), and the cotton effect corresponding to 592 nm was attributed to the induced chirality of RhB. The interaction between the TA and fluorescent molecules is further confirmed by IR spectra. As shown in **Figure S7**, the characteristic peaks of the carbonyl stretching vibrations of the RhB/TA assemblies are significantly broader from 1650 cm^{-1} to 1800 cm^{-1} and shifted towards higher wavenumbers 1725 cm^{-1} compare to RhB (1720 cm^{-1}). Moreover, the carboxyl peak of the RhB/TA assemblies (3180-3600 cm^{-1}) is also significantly broader than RhB and TA. These results indicated the formation of hydrogen bonding between TA and the carboxyl group of RhB.

In addition, UV-vis spectroscopy was used to investigate the stacking arrangement of RhB molecules within the block copolymer. As shown in **Figure S8**, the characteristic peaks of RhB molecules in the composite films are significantly blue-shifted compared to the neat RhB molecules, from 576 to 562 nm, indicating a face-to-face stacking arrangement between the RhB molecules in the assembles. Further, vibrational circular dichroism (VCD) spectroscopy was used to check the chain conformation chirality. **Figure 3b** shows the VCD and IR information of the composite films, where the induced chiral information of LC-BCP and RhB partially overlap with three parts (1) the chiral bands of the carbonyl group of the polymer ester group and the aromatic carboxyl group in RhB at 1768-1640 cm^{-1}, (2) the backbone vibration of the azobenzene functional group and the aromatic ring at 1620-1358 cm^{-1} showing strong chiral signals, (3) the asymmetric stretching vibration of the C-O-C bonds in LC-BCP and the stretching vibrations of Ar-O-Ar in RhB backbone was observed at 1115-1283 cm^{-1}. In particular, the 1345-1285 cm^{-1} stretching vibrational peak of the amino group in RhB shows a clear mirror image signal, which is strong evidence for the helical arrangement of the RhB molecule within the assembles. Based on these results, the induced chirality of the RhB molecule is generated through a combination of TA and RhB hydrogen bonding, and the

synergistic effect of the helical template induced π–π stacking. Transmission electron microscopy (TEM) is a powerful tool for observing microphase separation in block copolymers and is often used to identify phase chirality. To distinguish the different phases, PEO is stained with RuO4, which is dark in the image, and PMM (Azo) is the bright part. As shown in **Figure 3c** and **Figure S9**, PEO shows a large range of regular helical structures and the helical phases are consistent with the molecular chirality, with D-TA inducing a left-handed helical structure and L-TA inducing a right-handed helical structure. These results suggest that hydrogen bonding, π-π stacking, and liquid crystal self-organization are important driving forces for the hierarchical chiral transfer and induce the helical stacking of chain segments to form macroscopic chiral structures (**Figure 3c**).

To further investigate the differential chirality between the block copolymer assemblies and the homopolymer systems, CD spectra of homopolymer PMA(Azo)/TA/RhB composite films were analyzed. As shown in **Figure S10**, the mirror signals of azobenzene at 250 nm-550 nm, and chiral signals of RhB were observed at 580 nm. Then, the UV-vis characteristic peaks, CD signals and corresponding g_{abs} of the RhB in these systems were summarized in **Table S1**. Small molecules and homopolymer systems are incapable of microphase separation to induce the formation of large-scale ordered structures and local aggregation of chiral assemblies resulting in low chiral strength. Thus, in the above chiral system, the block copolymer acts as a chiral template to induce the helical order arrangement of achiral molecules. At the microscopic level, induced by the chiral molecules, ordered chiral structures were formed in the block copolymer, which led to chiral amplification; at the macroscopic level, increasing lamellae torsion, resulting in the formation of spherulites with large-scale spiral behavior.

2.3 Chiroptical switch properties

According to previous reports, controllable chiral arrangement of fluorescent molecules can endow the bulk films with CPL, and deformation of cis-trans isomerization of azobenzene group in response to external photothermal stimuli can be used as a chiroptical switch in the

film system.[36-38] As a result, it is possible to prepare CPL films with tunable properties in this work. Considering the UV light adsorption behavior of the azobenzene group, the light energy is dissipated as the transformation from trans to cis. Therefore, the excitation wavelength of the fluorescent molecule needs to avoid the UV band. Due to the large conjugated structure of the RhB molecule, higher wavelengths of excitation can be chosen based on its UV-vis spectrum and fluorescence excitation spectra (**supporting information Figure S11**). The chiral luminescence properties of the composite films were tested by CPL spectrometry. As shown in **Figure 4a**, the CPL signal was evident in the 560-680 nm for the LC-BCP/TA/RhB composite films, with a positive cotton effect for the L-TA-induced composite film and a negative cotton effect in D-TA and the g_{lum} up to 0.02 (**Figure 4b**). This is direct evidence of controllable chiral arrangement of fluorescent molecules in the assembled system. To discuss the optical tunability of the film, the composite film was irradiated with 365 nm (150 mW cm^{-2}) UV light for 1 minute, the trans-azobenzene was transformed to cis-azobenzene, the helical assembly system was disrupted and the fluorescent molecules were locally aggregated to form exciton junctions resulting in non-radiative dissipation of energy.[39, 40] After thermal annealing again at 125 °C, the chiral assemblies of composite film were reconstructed and induced a helical arrangement of fluorescent molecules to recover the CPL signal, achieving in situ reversible modulation of the chiral optical properties (**Figure 4c and 4d**).

3. Conclusion

In conclusion, we have demonstrated a facile method for fabricating solid films with controllable macroscopic chiral spherulites and tunable CPL by co-assembly of fluorescent molecules and LC-BCP induced by chiral TA. Hydrogen bonding, π-π stacking, and liquid crystal self-organization are the driving forces for chiral transfer from molecular chiral to chain segment conformational chirality to helical phase, and then crystal growth direction helical stacking to form macroscopic chiral spherulites. The chiral liquid crystal field plays a decisive role in the development of spherical crystals. The composite films have tunable CPL properties,

which can be erased by irradiation with UV light and recovered after thermal annealing. This strategy achieves in situ reversible modulation chiroptical of thin films, which can also be extended to other functional molecules or polymers and provide a new avenue for the development of advanced chiral materials.

4. Experimental Section

4.1 Materials

Rhodamine B (RhB, TCI), Tetrahydrofuran (THF, Super Dry J&K Scientific), Rhein (Macklin), L-(+)-Tartaric Acid, D-(-)-Tartaric acid (J&K Scientific), Poly (ethylene oxide) monomethyl ether (PEO; M_n=5.2 kg mol^{-1}, Aldrich) was dried in vacuum. Homopolymer PMA (Azo) (Mn=2.3 kg mol^{-1}) and LC-BCP, PEO_{114}-PMA $(Azo)_{70}$ (M_w=35.0 kg mol^{-1}, PDI=1.25), was prepared according to our previous work.[35]

4.2 Preparation of chiral composite films

The LC-BCP, TA, RhB were dissolved in THF, respectively. After the solids were completely dissolved, the TA solution was added to the LC-BCPs solution at a certain molar ratio (TA: PMA (Azo) = 2:1) and stirred at room temperature overnight. Then, RhB was added to the above mixture solution at a molar ratio (RhB: PMA(Azo) = 1:9) and stirred again at room temperature. The solution was then filtered through a 0.45 μm polytetrafluoroethylene microporous membrane. An appropriate amount of the solution was applied dropwise on a clear quartz plate. After the solvent is naturally volatilized, the film was immediately annealed on a hot plate at liquid-crystal state temperature (125 °C).

4.3 Instrument information and method

Optical microscopy (OM). The optical and 3D images of the chiral crystals were obtained using metallurgical microscopy (MX4RT, SOPTOP) and 3D microscopy (VHX-7000, KEYENCE, Japan).

Differential scanning calorimetry (DSC) was performed on a Discovery DSC 250 instrument. The thermodynamic properties of the pure polymer films and composite films were characterized under a nitrogen atmosphere at a heating and cooling rate of 10 °C min^{-1}.

Circular dichroism (CD) spectra were acquired on a JASCO J-1500 circular dichroism spectrometer and the UV-vis spectra were recorded on a Shimadzu UV-2600 UV-vis spectrometer. The chiral films were prepared on clear quartz plate and then annealed at 125 °C.

Vibrational circular dichroism (VCD) spectra were acquired on a vibrational circular dichroism spectrometer (Chiral IR-2X) and the infrared spectra (IR) were recorded on a Thermofisher Fourier IS-5 transform spectrometer. The samples were dropwise to the BaF_2 substrate and the annealing conditions were the same as those used to prepare the CD film.

Circularly polarized luminescence (CPL) spectra were recorded in a clear quartz using a JASCO CPL-200 spectrometer. Fluorescence (FL) spectra were tested on a HITACHI F-7000.

Wide-angle X-ray diffraction (WXRD) measurements were performed on a Rigaku SmartLab X-ray diffractometer employing monochromatic Cu-Kα radiation at a scan rate of 6° min^{-1} and operating conditions of 40 kV. The film samples were the same as those used for CD measurements.

Transmission electron microscopy (TEM) were conducted on JEOL JEM 2100 TEM and JEM F200.The operated accelerating voltage at 200 kV. The annealed films were embedded in epoxy resin and cured overnight at 60 °C. Thin sections of ~150 nm for TEM were prepared using a Leica ultra-cut UCT microtome.

Acknowledgements

This work was financially supported by the National Natural Science Foundation of China (grant no. 21574081, 21975156 and 52233016).

Conflict of Interests

The authors declare no conflict of interests.

Supporting Information

Supporting Information is available from the Wiley Online Library or from the author.

Received: ((will be filled in by the editorial staff))
Revised: ((will be filled in by the editorial staff))
Published online: ((will be filled in by the editorial staff))

References

1. A. Scarangella, V. Soldan, M. Mitov, *Nat. Commun.* **2020**, *11*, 4108.

2. P. Kumar, N. G. Paterson, J. Clayden, D. N. Woolfson, *Nature* **2022**, *607*, 387-392.

3. E. Merljak, B. Malovrh, R. Jerala, *Nat. Commun.* **2023**, *14*, 1995.

4. S. J. Gerbode, J. R. Puzey, A. G. McCormick, L. Mahadevan, *Science* **2012**, *337*, 1087-1091.

5. H. Liu, B. Pang, R. Garces, R. Dervisoglu, L. Chen, L. Andreas, K. Zhang, *Angew. Chem. Int. Ed.* **2018**, *57*, 16323-16328.

6. Y. Yang, J. Liang, F. Pan, Z. Wang, J. Zhang, K. Amin, J. Fang, W. Zou, Y. Chen, X. Shi, Z. Wei, *Nat. Commun.* **2018**, *9*, 3808.

7. W. Jiang, Z.-b. Qu, P. Kumar, D. Vecchio, Y. Wang, Y. Ma, J. H. Bahng, K. Bernardino, W. R. Gomes, F. M. Colombari, A. Lozada-Blanco, M. Veksler, E. Marino, A. Simon, C. Murray, S. R. Muniz, A. F. de Moura, N. A. Kotov, *Science* **2020**, *368*, 642-648.

8. Y. Duan, X. Liu, L. Han, S. Asahina, D. Xu, Y. Cao, Y. Yao, S. Che, *J. Am. Chem. Soc.* **2014**, *136*, 7193-7196.

9. J. Yuan, X. Lu, Q. Li, Z. Lü, Q. Lu, *Angew. Chem. Int. Ed.* **2021**, *60*, 12308-12312.

10. S. Zheng, J. Han, X. Jin, Q. Ye, J. Zhou, P. Duan, M. Liu, *Angew. Chem. Int. Ed.* **2021**, *60*, 22711-22716.

11. J. Yuasa, T. Ohno, H. Tsumatori, R. Shiba, H. Kamikubo, M. Kataoka, Y. Hasegawa, T. Kawai, *Chem. Commun.* **2013**, *49*, 4604-4606.

12. W. Wu, W. Hu, G. Qian, H. Liao, X. Xu, F. Berto, *Materials & Design* **2019**, *180*, 107950.

13. V. K. Valev, J. J. Baumberg, C. Sibilia, T. Verbiest, *Adv. Mater.* **2013**, *25*, 2517-2534.

14. Y. Cheng, S. Liu, F. Song, M. Khorloo, H. Zhang, R. T. K. Kwok, J. W. Y. Lam, Z. He, B. Z. Tang, *Mater. Horiz.* **2019**, *6*, 405-411.

15. X. Gao, J. Wang, K. Yang, B. Zhao, J. Deng, *Chem. Mater.* **2022**, *34*, 6116-6128.

16.J. Zhang, Q. Liu, W. Wu, J. Peng, H. Zhang, F. Song, B. He, X. Wang, H. H. Y. Sung, M. Chen, B. S. Li, S. H. Liu, J. W. Y. Lam, B. Z. Tang, *ACS Nano* **2019**, *13*, 3618-3628.

17. X. Gao, B. Zhao, J. Deng, *Macromolecules* **2022**, *55*, 10618-10627.

18. A. G. Shtukenberg, Y. O. Punin, E. Gunn, B. Kahr, *Chem. Rev.* **2012**, *112*, 1805-1838.

19. J. Xu, B.-H. Guo, Z.-M. Zhang, J.-J. Zhou, Y. Jiang, S. Yan, L. Li, Q. Wu, G.-Q. Chen, J. M. Schultz, *Macromolecules* **2004**, *37*, 4118-4123.

20. M.-C. Li, H.-F. Wang, C.-H. Chiang, Y.-D. Lee, R.-M. Ho, *Angew. Chem. Int. Ed.* **2014**, *53*, 4450-4455.

21. Y. Li, H. Huang, Z. Wang, T. He, *Macromolecules* **2014**, *47*, 1783-1792.

22. H.-F. Wang, C.-H. Chiang, W.-C. Hsu, T. Wen, W.-T. Chuang, B. Lotz, M.-C. Li, R.-M. Ho, *Macromolecules* **2017**, *50*, 5466-5475.

23. D. Maillard, R. E. Prud'homme, *Macromolecules* **2006**, *39*, 4272-4275.

24. T. Wen, H.-Y. Shen, H.-F. Wang, Y.-C. Mao, W.-T. Chuang, J.-C. Tsai, R.-M. Ho, *Angew. Chem. Int. Ed.* **2015**, *54*, 14313-14316.

25. F. H. Schacher, P. A. Rupar, I. Manners, *Angew. Chem. Int. Ed.* **2012**, *51*, 7898-7921.

26. M. Stefik, S. Guldin, S. Vignolini, U. Wiesner, U. Steiner, *Chem. Soc. Rev.* **2015**, *44*, 5076-5091.

27. C.-C. Chao, C.-K. Chen, Y.-W. Chiang, R.-M. Ho, *Macromolecules* **2008**, *41*, 3949-3956.

28. W. Han, X. Liao, Q. Yang, G. Li, B. He, W. Zhu, Z. Hao, *RSC Adv.* **2017**, *7*, 22515-22523.

29. M. Khorloo, X. Yu, Y. Cheng, H. Zhang, S. Yu, J. W. Y. Lam, M. Zhu, B. Z. Tang, *ACS Nano* **2021**, *15*, 1397-1406.

30. Q. Li, X. Lu, Z. Lv, B. Zhu, Q. Lu, *ACS Nano* **2022**, *16*, 18863-18872.

31. I. Song, J. Ahn, H. Ahn, S. H. Lee, J. Mei, N. A. Kotov, J. H. Oh, *Nature* **2023**, *617*, 92-99.

32. L. Gránásy, T. Pusztai, T. Börzsönyi, J. A. Warren, J. F. Douglas, *Nat. Mater.* **2004**, *3*, 645-650.

33. B. Crist, J. M. Schultz, *Progress in Polymer Science* **2016**, *56*, 1-63.

34. L. Yao, J. J. Watkins, *ACS Nano* **2013**, *7*, 1513-1523.

35. J. Yuan, X. Lu, S. Zhang, F. Zheng, Q. Deng, L. Han, Q. Lu, *Macromolecules* **2022**, *55*, 1566-1575.

36. Y. Sang, J. Han, T. Zhao, P. Duan, M. Liu, *Adv. Mater.* **2020**, *32*, 1900110.

37. T. Miao, X. Cheng, H. Ma, Z. He, Z. Zhang, N. Zhou, W. Zhang, X. Zhu, *Angew. Chem. Int. Ed.* **2021**, *60*, 18566-18571.

38. X. Cheng, T. Miao, Y. Ma, X. Zhu, W. Zhang, X. Zhu, *Angew. Chem. Int. Ed.* **2021**, *60*, 24430-24436.

39. H. Ren, D. Chen, Y. Shi, H. Yu, Z. Fu, *Polym. Chem.* **2015**, *6*, 270-277.

40. L. Zhou, P. Retailleau, M. Morel, S. Rudiuk, D. Baigl, *J. Am. Chem. Soc.* **2019**, *141*, 9321-9329.

Aggregate Open Access WILEY

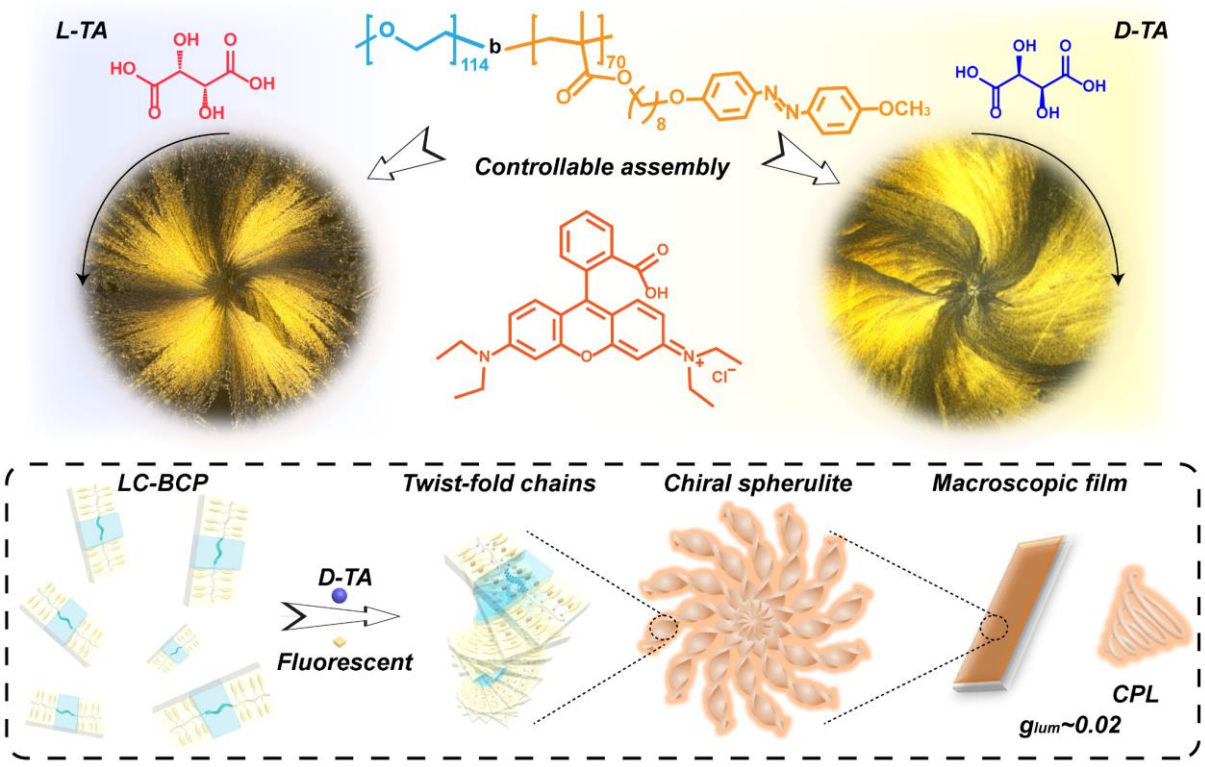

Scheme 1. Illustration of macroscopic chiral spherulites (ca. 1 mm) prepared by co-assembly of LC-BCP, RhB and chiral TA. The schematic shows the evolution of macroscopic chiral spherulites.

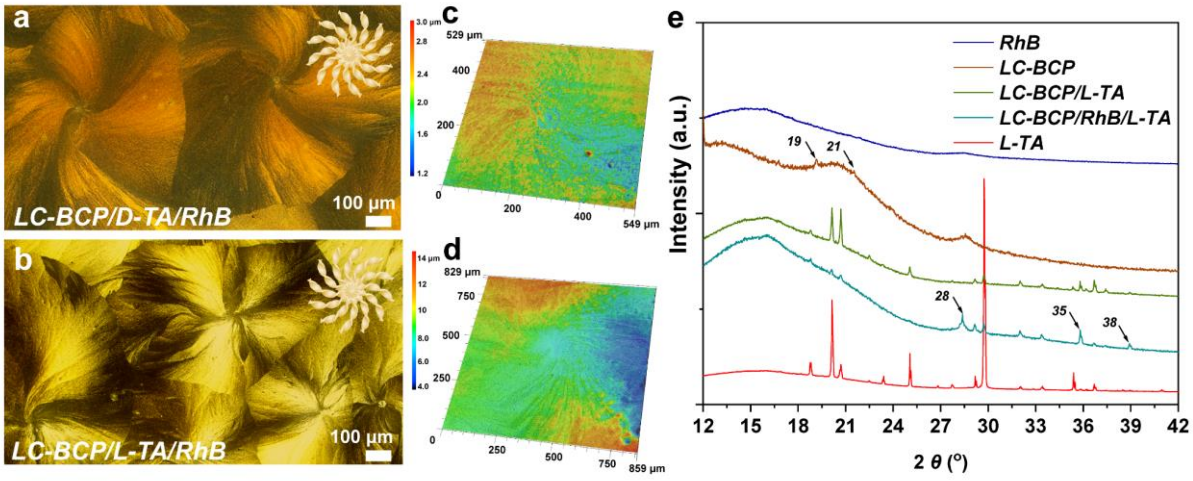

Figure 1. POM and 3D microscope images of LC-BCP/D-TA/RhB (a, c) and LC-BCP/L-TA/RhB (b, d), the molar ratio is TA: PMA (Azo) = 2:1, RhB: PMA(Azo) = 1:9. (e) XRD patterns of RhB, L-TA, LC-BCP, LC-BCP/L-TA and LC-BCP/L-TA/RhB.

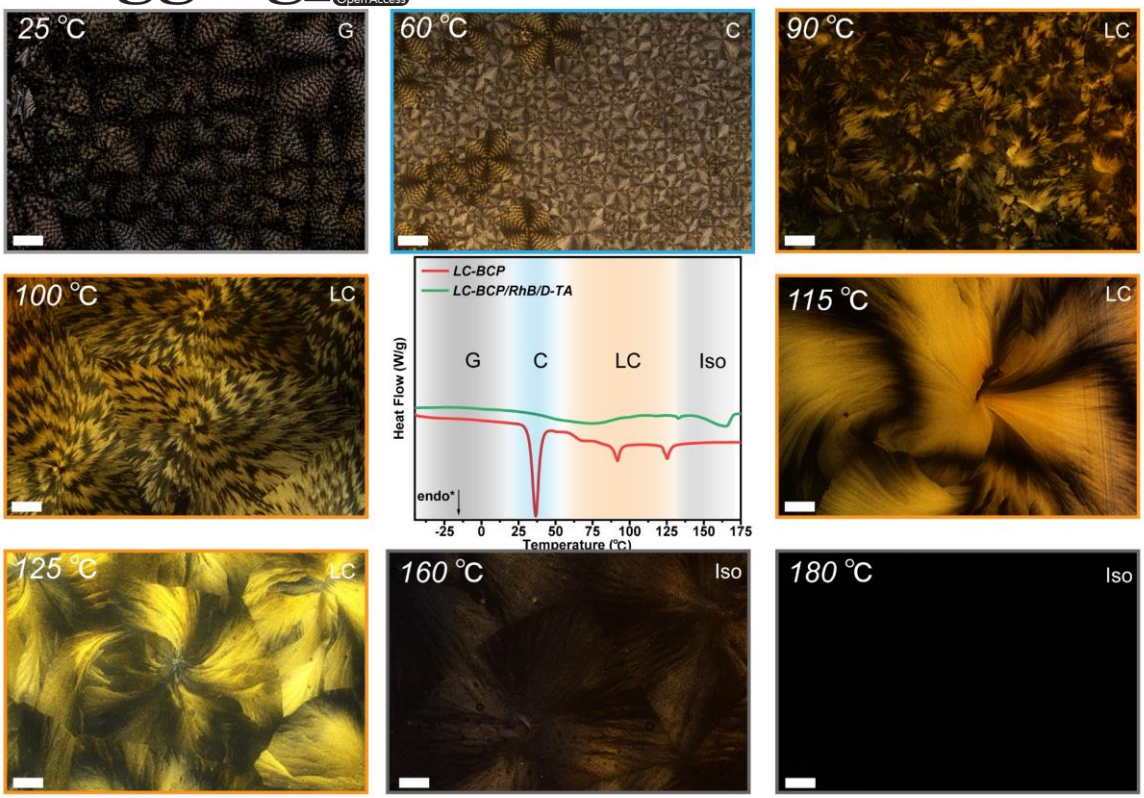

Figure 2. POM images of LC-BCP/D-TA/RhB film at different crystallization temperatures, scale bar is 100 μm. The middle graph shows the DSC curves of LC-BCP and LC-BCP/D-TA/RhB, C: crystalline range; G: glass transition; LC: liquid crystal phase; Iso: isotropic phase.

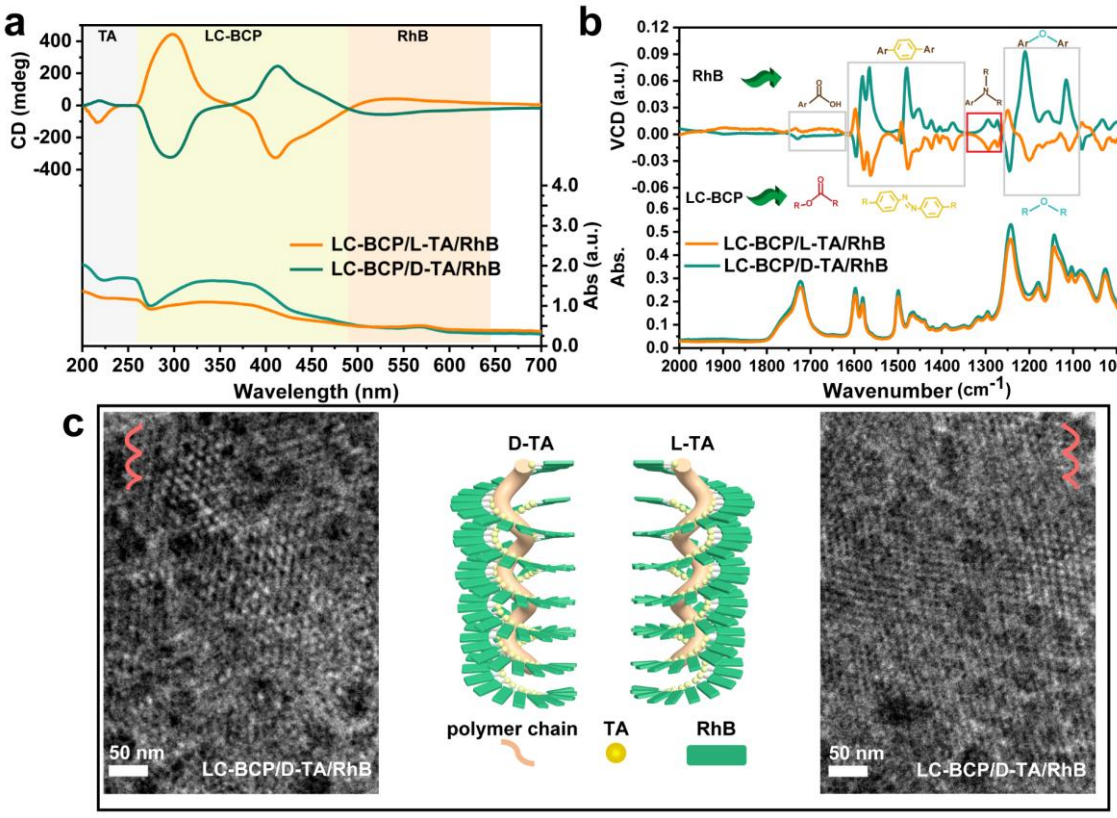

Figure 3. (a) CD spectra, (b) VCD spectra and (c) TEM images of LC-BCP/D-TA/RhB and LC-BCP/L-TA/RhB, respectively. The middle diagram represents a three-component assembly.

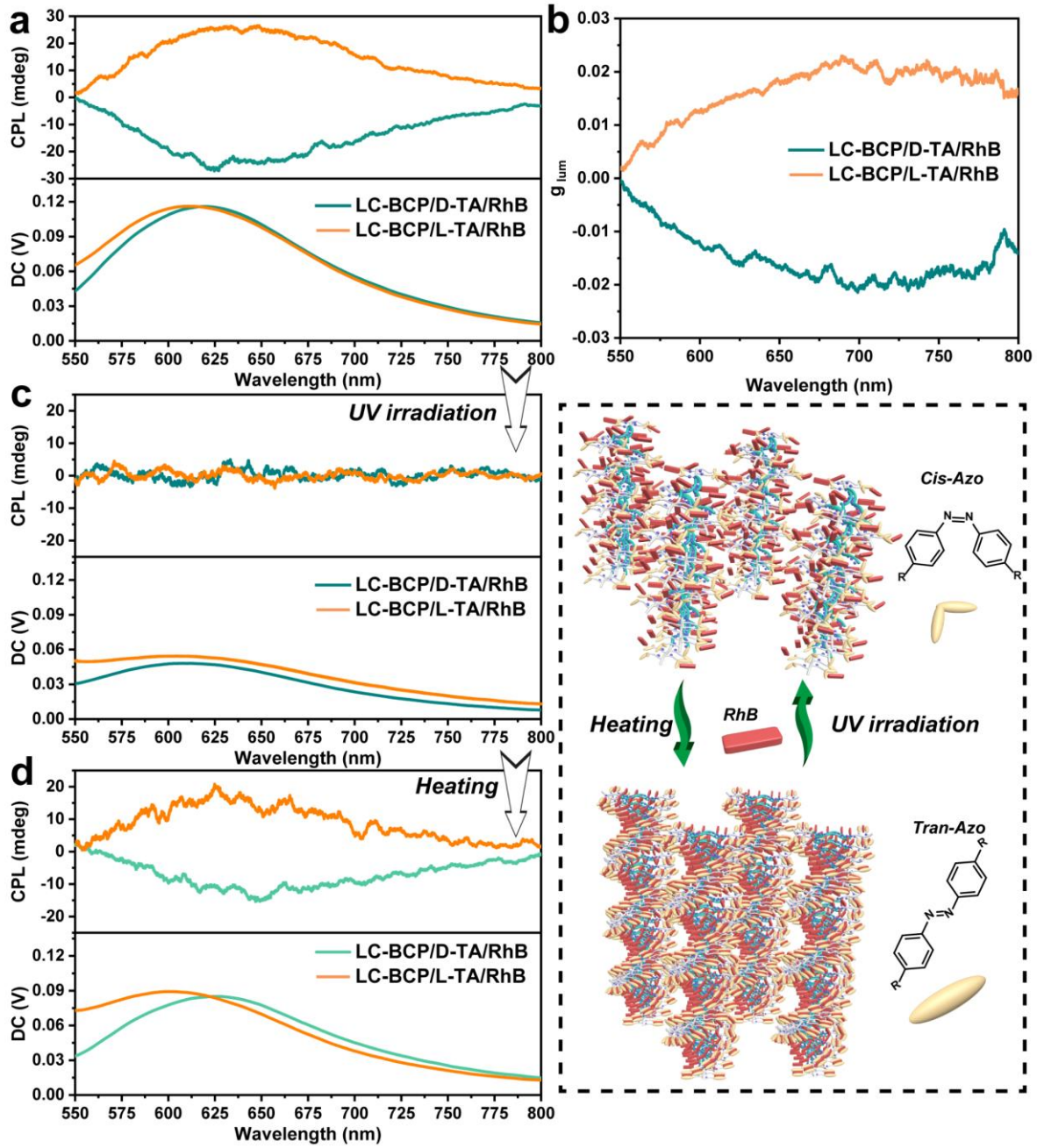

Figure 4. (a) CPL spectra and (b) g_{lum} spectra of LC-BCP/D-TA/RhB and LC-BCP/L-TA/RhB annealed film, Ex=530 nm. CPL spectra of chiral LC-BCP/TA/RhB film after UV irradiation (60 s, 365nm, 150 mW cm^{-2}) (c) and re-annealing (d). Scheme of the molecular and assembly structural changes induced by UV irradiation and thermal re-annealing.